Metabolism of N-methyl-amide by cytochrome P450s

Lionel Perrin, Nicolas Loiseau, François André, Marcel Delaforge

the FEBS Journal

Metabolism of *N*-methyl-amide by cytochrome P450s

Formation and characterization of highly stable carbinol-amide intermediate

Lionel Perrin[1,2,3,4], Nicolas Loiseau[5], François André[3,4] and Marcel Delaforge[3,4]

1 Université de Toulouse, Toulouse, France
2 CNRS-UMR 5215, Toulouse, France
3 CEA, iBiTecS, Service de Bioénergétique Biologie Structurale et Mécanismes (SB^{2}SM), Gif-sur-Yvette, France
4 CNRS-URA 2096, Gif-Sur-Yvette, France
5 Département de Pharmacologie, Laboratoire de Pharmacologie-Toxicologie INRA, Toulouse, France

Keywords
carbinol-amide; carbinol-amine; cytochrome P450; metabolism; tentoxin

Correspondence
M. Delaforge, CEA, iBiTecS-URA 2096 du CNRS, Service de Bioénergétique, Biologie Structurale et Mécanismes, CEA Saclay, F91191 Gif-sur-Yvette Cedex, France
Fax: +33 1 69 08 87 17
Tel: +33 1 69 08 44 32/68 39
E-mail: marcel.delaforge@cea.fr
L. Perrin, INSA, LPCNO, UMR 5215; 135 avenue de Rangueil, F-31077 Toulouse, France
Fax: +33 5 61 55 96 97
Tel: +33 5 61 55 96 64
E-mail: lionel.perrin@insa-toulouse.fr

(Received 29 March 2010, revised 4 April 2011, accepted 19 April 2011)

doi:10.1111/j.1742-4658.2011.08133.x

We report unambiguous proof of the stability of a carbinol intermediate in the case of P450 metabolism of an *N*-methylated natural *cyclo*-peptide, namely tentoxin. Under mild acidic or neutral conditions, the lifetime of carbinol-amide is long enough to be fully characterized. This metabolite has been characterized using specifically labeled ^{14}C-methyl tentoxin isotopomers, HPLC, HPLC-MS, MS-MS and NMR. Under stronger acidic conditions, the stability of this metabolite vanishes through deformylation. A theoretical mechanistic investigation reveals that the stability is governed by the accessibility of the nitrogen lone pair and its protonation state. For carbinol-amines, even in neutral conditions, the energy barrier for deformylation is low enough to allow rapid deformylation. Carbinol-amide behaves differently. Under neutral conditions, delocalization of the nitrogen lone pair increases the energy barrier of deformylation that is a slow process under such conditions. After protonation, we were able to optimize a deformylation transition that is lower in energy and thus accounts for the lower stability of carbinol-amides observed experimentally in acidic conditions. Finally, by considering the protocol usually used for extraction and analysis of this type of metabolite, carbinol-amide may thus be frequently ignored in drug metabolism pathways.

Introduction

Numerous alkyl amines are present in our environment either as natural compounds or as chemically synthesized drugs. By contrast to secondary and, to a lesser extent, primary amines, tertiary amines are less polar, exhibit lower basicity and thus migrate more easily through cell membranes. Oxidative dealkylation is among the main metabolic pathways of such compounds. A large number of mechanistic studies deals with dealkylation processes catalyzed by enzymatic systems such as peroxidases or cytochrome P450s [1–4]. It is now accepted that *N*-dealkylation involves a multistep mechanism based on either proton or electron abstraction, followed by fixation of one activated oxygen atom [4–6], leading to a carbinol-amine intermediate.

In a metabolic scheme, this intermediate eliminates a molecule of aldehyde to produce a secondary amine. Identification and characterization of *N*-hydroxymethyl

Abbreviation
TTX, tentoxin.

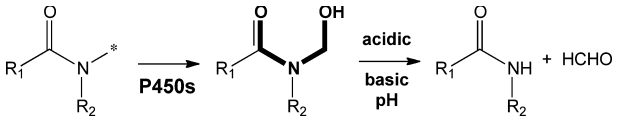

intermediates remains scarce and frequently speculative, in both *in vivo* and *in vitro* studies. Interestingly, *N*-hydroxymethyl derivatives have been reported as prodrug candidates, the active compound being the demethylated metabolite [7]. However, carbinol-amines or carbinol-amides P450 metabolites have been reported in the case of benzylic tertiary amine (clebopride **1** [8]), aromatic amines (*N*-methylcarbazole **2** [9–14] or nicergoline **3** [15–19]), dialkylated-aliphatic amides [20–22], cotinine **4** [23], dialkylated-aromatic amides (benzamide derivatives [24,25] or triazolyl-benzophenone derivatives **5** [26]), *N*-methyl-imide (*N*-methylphthalimide **6** [7]) or *N*-substituted urea derivatives (ritonavir **7** [27]). The chemical structures of these molecules are given in Scheme 1. For these compounds except compound **1**, the *N*-hydroxymethyl function seems to be stabilized by delocalization of the nitrogen lone pair to an adjacent carbonyl or aromatic groups.

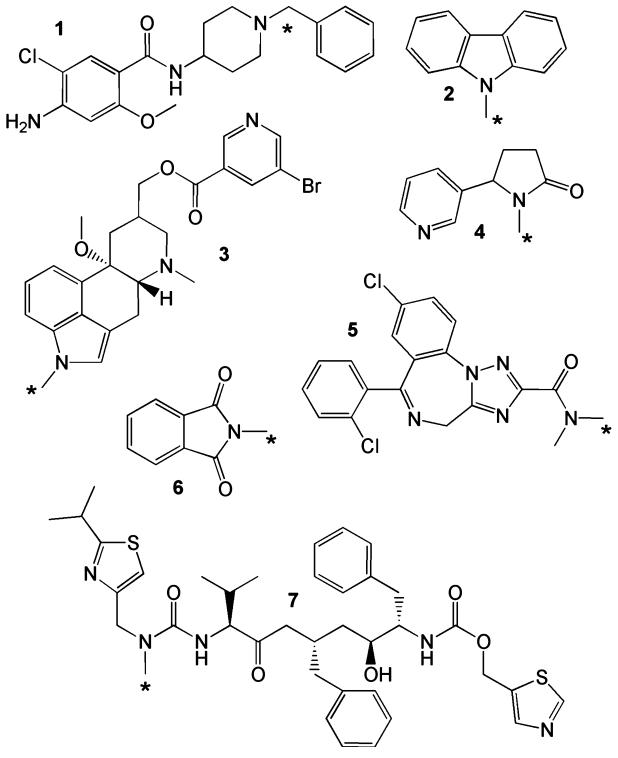

Scheme 1. Example of known compounds whose carbinol-amine (**1–3**) or carbinol-amide (**4–7**) type of metabolites has been identified. Stars label sites of hydroxylation. **1**, clebopride; **2**, *N*-methyl-carbazole; **3**, nicergoline; **4**, cotinine; **5**, 5-[(2-aminoacetamido)methyl]-1-[4-chloro-2-(*o*-chlorobenzoyl)phenyl]-*N*,*N*-dimethyl-1*H*-1,2,4,-triazole-3-carboxamide; **6**, *N*-methyl-phtalimide; **7**, ritonavir.

To date, carbinol-amide intermediates have not been identified in the metabolism of *N*-methylated peptides or *cyclo*-peptides. There is only one suggestion concerning the formation of an *N*-hydroxymethyl intermediate during fish metabolism of cyclosporine A [28].

Here, we show, through the example of tentoxin (TTX), that such intermediates may occur more regularly than reported in the metabolism of natural *N*-methylated cyclopeptides. TTX [cyclo-(L-*N*-MeAla^1-L-Leu^2-*N*-Me(Δ*Z*)Phe^3-Gly^4] (Scheme 2) is a natural hydrophobic cyclotetrapeptide which acts in certain plant species as a noncompetitive inhibitor of chloroplast ATP-synthase [29–31], provoking chlorosis. We have previously shown that TTX is efficiently metabolized through *N*-demethylation by mammal cytochrome P450 [32]. In order to gain insight into the P450 metabolism mechanism of *N*-Me-cyclo-peptides, the metabolism of a set of molecules composed of TTX (**8a**), *iso*-TTX (**8b**) and dihydrotentoxin (**9**) was studied in detail. Because the two *N*-Me groups of TTX may be implied in the metabolic scheme, and a filial relationship may exist between metabolites, we implemented the following strategy: (a) numeration, quantification and isolation of metabolites starting with both natural and ^{14}C-radiolabeled substrates using HPLC; (b) structural identification of metabolites by HPLC/MS and MS-MS, and NMR spectroscopy; (c) demonstration of the relationship between metabolites via a stability study involving ^{14}C-isotopomers of metabolites; and (d) investigation of the chemical mechanism involved in the metabolite cascade. This mechanistic study was carried out on a series of model compounds that share functional similarities with known *N*-methylated substrates undergoing deformylation through P450s metabolism (Scheme 1).

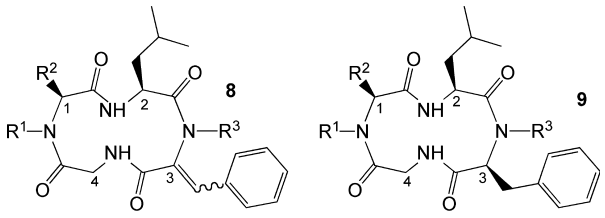

Scheme 2. Chemical structure of tentoxin cyclo-(L-*N*-MeAla^1-L-Leu^2-*N*-Me(Δ*Z*)Phe^3-Gly^4) and its used analogs.

Results

In vitro experiments and analysis

The metabolism of TTX yields two main metabolites, M1 and M2, which are characterized by two distinct HPLC retention times (Fig. 1A). Metabolite M1 forms predominantly at short incubation times and is characterized, on reverse-phase columns, by a higher retention time than M2. Incubation of TTX with different liver mammalian microsomes including rat, mice, rabbit, cow, sheep or human, produces a mixture of these two metabolites. Table 1 shows the data obtained in rat liver microsomes. It appears that dexamethasone-pretreated rat liver microsomes are the most active in metabolizing TTX [32]. In all conditions, 10 min of incubation selectively produces M1 over M2 with M1/M2 ratios > 1. These M1/M2 ratios decrease significantly, as shown by comparison of the incubation extracts when analyzed after at least 24 h preparation in the absence of proteins. In 30 min or 1 h incubations, M1 disappears in favor of M2 (dexamethasone-treated rat microsomes). The M1/M2 ratio was also found to be pH dependent, decreasing from 2.0 to 1.6 and 0.18 for pH values of 6.8, 7.4 and 8.2, respectively.

Preliminary attempts to determine the structure of M1 and M2 using routine protocols revealed that: (a) isolated M1 and M2 both displayed apparent molecular masses of 400 Da and identical MS fragmentation schemes; (b) HPLC analysis of the separated and purified metabolites M1 and M2 led to a single peak corresponding to M2 that fits with the HPLC retention time and MS cleavage of Ala^1-TTX; and (c) the relative amounts of M1 and M2 were different depending on the acidity of the HPLC eluent or on the time elapsed between incubation and analysis. In order to delineate the structural differences between these two metabolites, ^{14}C labeling was used at the two sites of the molecule that are potentially *N*-demethylated.

Radiolabeling experiments

1-*N*-Me and 3-*N*-Me ^{14}C-labeled isotopomers were synthesized and used independently. For both isotopomers, M1 is labeled in all incubations, which demonstrates that the ^{14}C methyl group is not eliminated (Fig. 1B,C). When the *N*-Me of residue Ala^1 is ^{14}C-labeled, M2 is not apparent on the radiochromatogram (Fig. 1B). This proves that *N*-demethylation occurred on residue 1. By contrast, when the *N*-Me of residue 3 [Δ(*Z*)Phe] is ^{14}C-labeled, M2 radioactivity is detectable (Fig. 1C). This demonstrates that [Δ(*Z*)Phe] is not involved in the biotransformation process. Finally, after fraction collection, concentration under heating and analysis by HPLC, the sample that initially contained M1 exhibits the same features as M2. This validates the filial relationship between M1 and M2, and shows that M2 originates from M1.

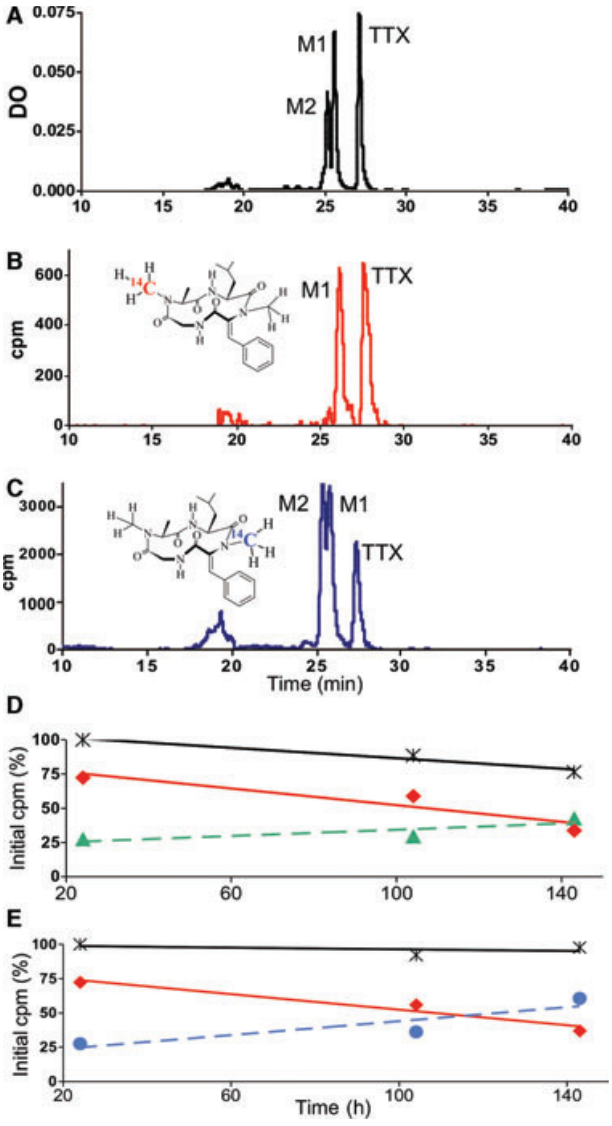

Fig. 1. (A) HPLC separation of tentoxin metabolites using UV detection at 280 nm. (B) Radiochromatogram of an incubation performed using tentoxin isotopically labeled on residue 1 (^{14}C-*N*-Me-Ala^1-TTX). (C) Radiochromatogram of an incubation performed using tentoxin isotopically labeled on residue 3 (^{14}C-*N*-Me-ΔPhe^3 TTX). (D) Time-dependent evolution of labeled metabolites of ^{14}C-*N*-Me-Ala^1-TTX in 50% phosphate buffer pH 7.4/50% acetonitrile solution at 4 °C. (E) Time-dependent evolution of labeled metabolites of ^{14}C-*N*-Me-ΔPhe^3-TTX in 50% phosphate buffer pH 7.4/50% acétonitrile solution at 4 °C. (✱) Total recovered radioactivity, (◆) M1 metabolite; (▲) front solvent, (●) M2 metabolite.

Table 1. Amounts of metabolites M1 and M2 recovered after 10 min incubations of 100 μM tentoxin using 1 μM of rat microsomal preparations and an NADPH-generating system. Analyses were performed at room temperature either in < 6 h or 1 day after incubation time.

	10 min incubations, analysis after incubation			10 min incubations, analysis after 24 h		
Microsomal preparation	M1 (μM)	M2 (μM)	M1/M2	M1 (μM)	M2 (μM)	M1/M2
Untreated rat	16.0	6.8	2.35	10.5	12.0	0.86
Rat DEX	23.0	14.0	1.64	15.0	25.0	0.60

Stability study

Storage and stability of M1

Table 1 shows analysis of the samples after incubation and after 1 day storage at room temperature in a mixture of 50% phosphate buffer/50% acetonitrile, in the absence of microsomal proteins. The total amount of metabolites M1 + M2 appears constant, indicating that M1 decreases in favor of M2. M1 was collected after HPLC analysis performed using a water/acetonitrile linear gradient and was subjected to various storage conditions at 4 °C. In a 50/50 (v/v) water/acetonitrile mixture or in acidic conditions (50/50 v/v water/acetonitrile plus 0.1% formic acid, or 50/50 v/v phosphate buffer pH 5.6/acetonitrile), the amount of M1 decreases slowly, with a half-life > 50 h, as shown by the radioactive decay of 1-*N*-Me-^{14}C-TTX (Fig. 1D). M1 displays the same stability after removal of acetonitrile under nitrogen gas. Reversely, addition of phosphate or Tris buffer (pH 7.4 or 8.2), with or without acetonitrile as a solvent, leads to a complete transformation of M1 into M2 in ~ 20 h (Fig. 2A,B). The conversion is complete in < 20 min at pH 10. By contrast, lyophilized M1 is stable for a few months at −80 °C.

Radioactive isotopomers breakdown

Ther metabolism of both radioactive isotopomers yields similar results and gives additional information concerning M1 radioactive decay. Metabolism of ^{14}C-TTX labeled on the *N*-Me of residue Ala^1 converts to radioactive M1 (Fig. 1B), whereas only a trace of M2 is detected (UV detection). During storage at room temperature, M1 radioactivity decreases slowly, whereas front peak radioactivity increases. The front solvent radioactive peak contains polar compounds such as formaldehyde. Total radioactivity decreases by ~ 20% over a period of 6 days at 4 °C (Fig. 1D).

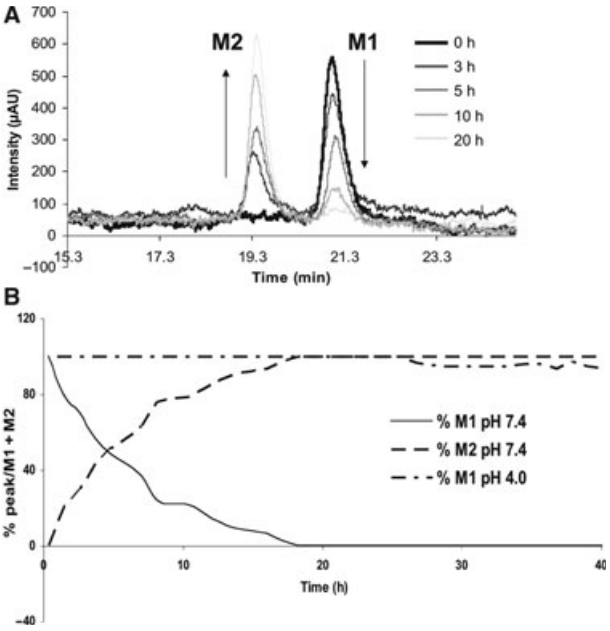

Fig. 2. Time-dependence evolution of purified M1 converting to M2 as a function of time and storage conditions. (A) HPLC peak of purified M1 and its evolution to M2 as a function of storage time in 50% phosphate buffer (pH 7.4)/50% acetonitrile. (B) Time course of M1 (dot-hashed line) stored in 49.9% water/50% acetonitrile/0.1% formic acid (pH 4) and co-evolution of M1 (plain line) and M2 (dashed line) stored in 50% phosphate buffer (pH 7.4)/50% acetonitrile.

Metabolites of ^{14}C-TTX labeled on the *N*-Me of residue ΔZ-Phe^3 contain mainly radioactive M2 (Fig. 1C) and no significant amounts of radioactive compounds in the front solvent peak. During storage, the radioactivity signal of M1 decreases, whereas that of M2 increases, without formation of new radioactive peak (Fig. 1E). In this case, the total radioactivity of the M1 + M2 peaks remains constant for 6 days at 4 °C.

Structural identification of metabolites

Mass spectrometry

The MS spectrum under a water/acetonitrile gradient of the M1 molecular peak in positive and negative mode almost corresponds to that of M2 (*m/z* 399 in the negative mode and *m/z* 401 in the positive mode), and exhibits the same mass spectrum as the authentic Ala^1-TTX (spectra not shown). The highest MS signals are obtained in the presence of acetic acid and allow the detection of different adducts of M1, in negative or positive modes (Table 2 and Fig. 3). In the negative mode, *m/z* at 399, 411, 429, 465, 467 and 489 are observed (Fig. 3A). The MS-MS spectrum of *m/z* 429 leads to fragments at *m/z* 411 (loss of H_2O), 381 (loss

Table 2. MS and MS-MS fragments of M1 TTX metabolite (in bold) and tentative assignment of loss of fragments obtained after HPLC-MS ESI in positive and negative modes.

Negative ionization mode		Positive ionization mode	
MS^-	$MS\text{-}MS^-$	MS^+	$MS\text{-}MS^+$
399	**381** (–18)	**413**	**356** (–57)
M – H (–30)	$-H_2O$	M + H – H_2O	$-C_2H_3NO$
$-CH_2O$	**355** (–44)		**342** (–71)
	$-CH_2NO$		–Ala
	289 (–110)		**217** (–196)
	271 (–128)		(NMe-ΔPhe-Gly)$^+$
429	**411** (–18)	**431**	**328** (–103)
M – H	**381** (–30, –18)	M + H	$-C_3H_5NO_3$
	311 (–118)		**318**(–113)-Leu
465, 467	**435, 437** (–30)	**453**	**423** (–30)
M – H + HCl	**399** (–30, –36)	M + Na	
489	**459** (–30)	**469**	**439** (–30)
M – H +	**441** (–30, –18)	M + K	
CH_3CO_2H	**429** (–60)		
	399 (–60, –30)		

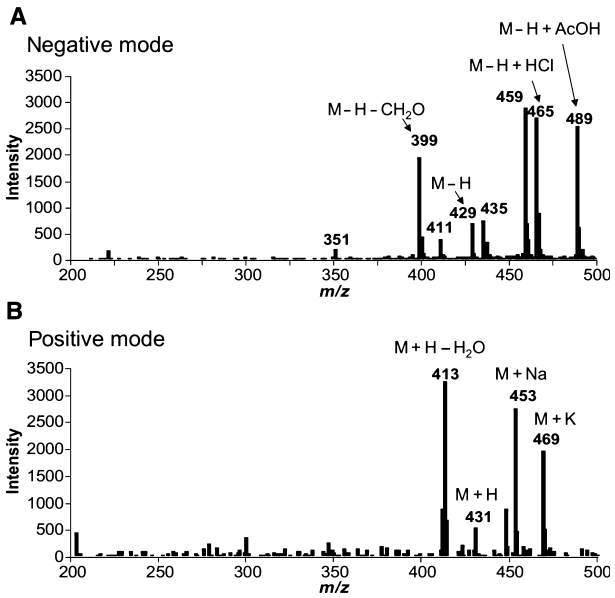

Fig. 3. Mass spectrometry of the M1 TTX metabolite obtained either in negative (A) or positive (B) ESI mode realized upon addition of 0.1% acetic acid to eluent A (see Materials and methods). The M1 TTX metabolite was obtained from a 10 min incubation of TTX using dexamethasone-treated rat microsomes in the presence of an NADPH-generating system.

of H_2O and CH_2O) and 311 (Table 2), whereas fragmentation of *m/z* 465 and 467, which are in a ratio of 3:1, led to 30 amu loss. The signal at *m/z* 489 leads to fragments at *m/z* 459 (loss of CH_2O), 441 (loss of CH_2O and H_2O), 429 (loss of AcOH) and 399 (loss of AcOH and CH_2O). This fragmentation scheme corresponds to an hydroxy metabolite of TTX with a molecular peak at *m/z* 429 (TTX + 'O'–'H') that forms a chlorine (*m/z* at 465 and 467 in a ratio of 3:1) or an acetic acid adduct (*m/z* at 489) in the MS source. The MS signal at *m/z* 399 and the fragments observed under collision (losses of 30 amu) agree with cleavage of the CH_2O fragment. Under the same HPLC conditions, using the positive ionization mode (see Fig. 3B and Table 2), the mass spectrum shows fragments at 413, 431, 453 and 469. Both *m/z* at 453 $(M + Na)^+$ and *m/z* at 469 $(M + K)^+$ conducted under collision lead to 30 amu losses, whereas the 413 collision leads predominantly to fragments at *m/z* 356 (−57), 342 (M-Ala) and 217 (M-*N*-Me-ΔPhe-Gly).

Carbinol-amide formation is not restricted to TTX and is also observed in the metabolism of TTX analogs such as *iso*-TTX and dihydro-TTX (Scheme 2), which differ from TTX by isomerization or saturation of the α,β-dehydrogenated bond of residue Δ(*Z*)Phe[3], respectively (data not shown).

NMR analysis

A proton NMR spectrum was recorded in $CDCl_3$ at room temperature on a mixture of M1 and M2, and was analyzed in the 3 p.p.m. region characteristic of *N*-methyl proton resonances of the cyclo-peptide (Fig. 4). The spectrum of pure intermediate M1 cannot be obtained because of the continuous conversion to M2. At room temperature in $CDCl_3$, TTX is in fast

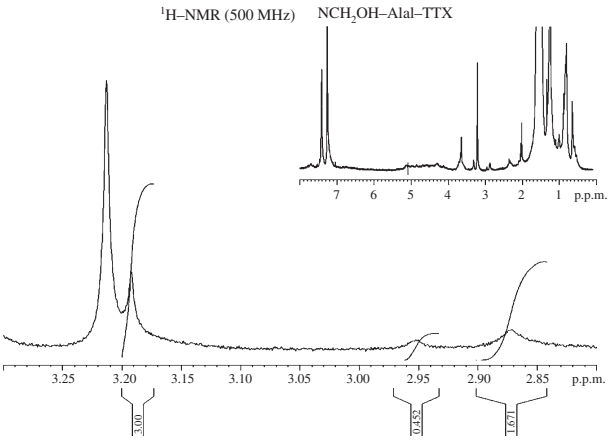

Fig. 4. *N*-Me protons region of 500.13 MHz proton NMR spectrum of metabolite M1 partially converted into metabolite M2 recorded in $CDCl_3$ at 300 K, TMS was used as an internal reference of chemical shift. No pH or temperature correction was used. The inset shows the entire spectrum.

exchange between the two main conformers A and B [33,34], and shows two *N*-methyl peaks (*s*, 3H), one around 3.2 p.p.m. for *N*-Me-ΔPhe protons, and one around 2.9 p.p.m. for *N*-Me-Ala protons. As expected, the *N*-methyl peak at 2.9 p.p.m. is absent in authentic Ala-TTX (M2) (spectra not shown). In the spectrum of TTX metabolites, a mixture of *N*-methyl peaks is observable. This corresponds to a mixture of demethylated metabolite (M2, Ala-TTX) and carbinol-amide intermediate (M1). The latter should exhibit a (*s*, 2H) peak instead of a (*s*, 3H) peak in the 2.9 p.p.m. region. The area ratio of resonances matches the following final assignment. The major peak at 3.22 p.p.m. is assigned to *N*-Me protons of ΔPhe residue in the *N*-demethylated compound (M2). The other peaks (3.19, 2.95, 2.87 p.p.m.) belong to metabolite M1 and are found in a consistent ratio after integration: (2.87 + 2.95 p.p.m) = 2/3 × 3.19 p.p.m. The peak at 3.19 p.p.m (*s*, 3H) corresponds to the *N*-Me on residue 3, whereas peaks at 2.87 and 2.95 p.p.m belong to the methylene protons of residue 1 NCH_2OH group, in two different conformers. Conformational analysis performed, as previously published [35], suggests two possible stable conformations of the *N*-hydroxymethyl group (above the average plane of the ring, or under), which give rise to two different conformers of M2 in a 75% (2.87 p.p.m)/25% (2.95 p.p.m) ratio. Taken together, these data converge to denote the assignment of the carbinol-amide function on residue 1 to metabolite M1.

Computational study

In order to determine a plausible mechanism connecting M1 to M2 and to assess the factors that govern the stability of carbinol-amide and carbinol-amine, we initially computed the thermodynamics of the formation of the hydroxy metabolite via Equation (1). This was carried out for a set of model compounds (Scheme 3) that share most of the structural diversity observed in the P450s *N*-methylated substrates presented in Scheme 1. Because Equation (1) is a model transformation, its absolute free enthalpy is not relevant, whereas the trend in thermodynamics might point out differential effects. The free enthalpy of reaction of the subsequent formaldehyde elimination (Equation 2) has been also computed. The data are shown in Table 3.

$$R^1R^2NCH_3 + H_2O_2 = R^1R^2NCH_2OH + H_2O \quad (1)$$

$$R^1R^2NCH_2OH = R^1R^2NH + HCHO \quad (2)$$

Table 3 reveals that the structure of the substrate has almost no influence on the energetics of the reactions shown in Equations (1) and (2). The presence or absence of an intramolecular hydrogen bond in the carbinol-amide derivatives does not modify the results, these two configurations (with or without hydrogen bond) are isoenergetic. Finally, C-hydroxylation is more favorable than N-oxidation; for *N*,*N*-dimethylethanamine (**a**) and *N*,*N*-dimethylacetamide (**d**), C-hydroxylated compounds are more stable by 43 and 63 kcal·mol^{-1}, respectively.

As the thermodynamics of the reactions in Equations (1) and (2) does not allow us to distinguish between the stability of carbinol-amines and carbinol-amides, this difference in behavior might originate from the relative height of the transition states involved in the elimination reaction. Based on reaction conditions, three types of mechanism can be considered: neutral, cationic and anionic. Because highly basic conditions are not realistic experimentally (pH buffered at 7.4), a mechanism involving deprotonation of the hydroxyl group of carbinol-amines or carbinol-amides cannot operate.

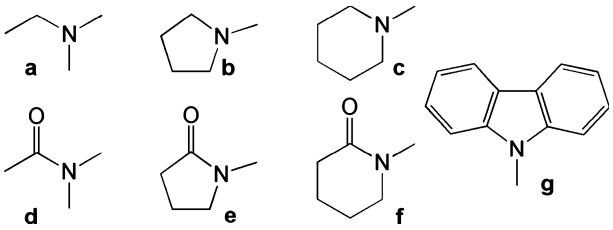

Scheme 3. Modeled compounds used for the molecular modeling study of the stability of carbinol-amines or carbinol-amides derivatives (**g** is compound **2** in Scheme 1).

Table 3. Thermodynamic Δ_rG(CPCM) and kinetic $\Delta_rG^{\#}$(CPCM) data associated to the monohydroxylation [reaction (1)] and elimination [reaction (2)] of model *N*-methyl-amines and *N*-methyl-amides **a**–**g** (Scheme 3).

	Monohydroxylation reaction (1)	Elimination reaction (2)	
	Δ_rG^a (kcal·mol^{-1})	Δ_rG^a (kcal·mol^{-1})	$\Delta_rG^{\#b}$ (kcal·mol^{-1})
a	−63.6	−41.3	29.9
b	−68.3	−43.0	32.8
c	−65.9	−40.6	31.9
d	−67.9	−43.8	51.9
e	−65.8	−39.5	55.3
f	−67.6	−41.5	54.2
g	−63.5	−40.5	51.0

[a] Relative energy computed relatively to the initial separated reactant ($R^1R^2NCH_3 + H_2O_2$). [b] Relative energy computed relatively to the $R^1R^2NCH_2OH$ intermediate (carbinol-amine or carbinol-amide). Energies and free enthalpies are given in kcal·mol^{-1}.

Under neutral conditions, a one-step concerted mechanism of formaldehyde elimination can be drawn. The relative free enthalpy of activation ($\Delta_r G^{\#}$) for this reaction has been computed for the entire set of modeled compounds (Table 3). In the amide series, no transition state of elimination involving the carbonyl function can be found on the potential energy surface. Two groups of values from Table 3 should be highlighted: the barriers for the deformylation of carbinol-amines are ~ 30 kcal·mol^{-1}, whereas the reaction requires 53 kcal·mol^{-1} to proceed for carbinol-amides and *N*-hydroxymethylcarbazole. Although the barriers are high, this trend is not surprising because this mechanism implies the participation of the nitrogen lone pair, which is free in carbinol-amines and partially delocalized in the peptide bond in carbinol-amides or in the vicinal aromatic rings in *N*-hydroxymethylcarbazole. Finally, cyclic constraints have marginal effects on the kinetics of the elimination reaction. In order to obtain more realistic energy barriers, assistance by a water molecule has been considered. In this case, the reaction relies on a six-membered ring in which the water molecule acts as a proton relay [36,37]. For carbinol-amine **a** and carbinol-amide **b**, the barriers decrease to 16 and 29 kcal·mol^{-1}, respectively. These results show that, under neutral conditions, carbinol-amines can easily undergo deformylation, whereas the high barrier significantly slows deformylation of carbinol-amides.

Under acidic conditions, a cationic mechanism in which the first step corresponds to the protonation of carbinol-amines or carbinol-amides has been considered. Because the carbinol-amines and carbinol-amides modeled to date behave similarly, the mechanism has only been computed for *N*,*N*-dimethylethanamine (**a**) (Scheme 4A) and *N*,*N*-dimethylacetamide (**d**) (Scheme 4B). Protonated molecules are used as references in energy profiles.

The most favorable protonation of *N*-methyl-*N*-hydroxymethyl-ethanamine takes place on the nitrogen. Oxonium **a2** and iminium **a3** are less favorable by 6 and 18 kcal·mol^{-1}, respectively. **a1** eliminates protonated formaldehyde through transition state **a4**. A free enthalpy barrier of 53 kcal·mol^{-1} is required to reach this transition state. This transition state directly yields $EtMeNH_2^+$ (**a5**) and formaldehyde. The free enthalpy of reaction for this elimination reaction is 23 kcal·mol^{-1}. This thermodynamic balance originates from the higher basicity of tertiary amine than secondary amine in the gas phase. This trend in basicity is reversed in solution; and the reaction should be favorable in solution. Finally, the increase in the energy barrier between the neutral and the cationic cases is explained by loss of the amine lone pair that plays a major role in the elimination process. Despite our efforts, no deformylation transition state assisted by a water molecule could be optimized in this case.

The mechanism computed for the deformylation of *N*-methyl-*N*-hydroxymethyl-acetamide is reported in Scheme 4B. The most favorable protonation site of the carbinol-amide is the O–carbonyl atom (**d4**). This O-carbonyl protonated intermediate can evolve through a deformylation transition state (**d6**) leading to O-protonated *N*-methyl-acetamide (**d7**) and formaldehyde via a of barrier of 53 kcal·mol^{-1} and a free enthalpy balance of 24 kcal·mol^{-1} with respect to intermediate **d4**. It is noteworthy that this barrier and the thermodynamic balance are reduced to 21 and 8 kcal·mol^{-1}, respectively, thanks to the assistance of a water molecule, and make the reaction possible under mild conditions.

Alternative routes that involve N-amide protonation (**d1**) undergo deformylation through transitions states **d5** or **d5′**. From **d4**, the free enthalpy barriers to reach **d5** and **d5′** are 44 and 33 kcal·mol^{-1}, respectively. Structurally, transition state **d5′** is the analog of transition state **a4** and, as mentioned for the later, we failed to decrease the barrier by adding explicit water molecules. Interestingly, transition state **d5** shows reasonable cyclic constraints without the assistance of a water molecule. In a nonaqueous media, deformylation should slowly occur via this transition state.

Discussion

In vitro incubations of TTX and some of its analogs, using microsomal liver preparations of rat pretreated with dexamethasone, mainly produce two metabolites, M1 and M2. The nature and structure of these metabolites have been unambiguously assigned using HPLC-MS, MS-MS and NMR. Because a methyl or hydroxymethyl transposition during incubation, storage or MS analysis cannot explain the identical molecular masses and fragmentation scheme of M1 and M2, the *N*-Me groups of TTX have to be distinguished. ^{14}C-specific radioactive isotopomers have been fruitfully used for this purpose. This set of experiments shows that metabolism occurs specifically on the *N*-Me groups of TTX residue 1 and conducts to a carbinol-amide intermediate. Direct observation of stable *N*-hydroxyalkyl metabolites is noteworthy because their report remains scarce in the case of secondary or tertiary amine or N,N-dialkylated amide. A possible carbinol-amide metabolite was suggested in the case of fish cyclosporin A metabolism, but its identification remained speculative [28]. Our data give, for the first

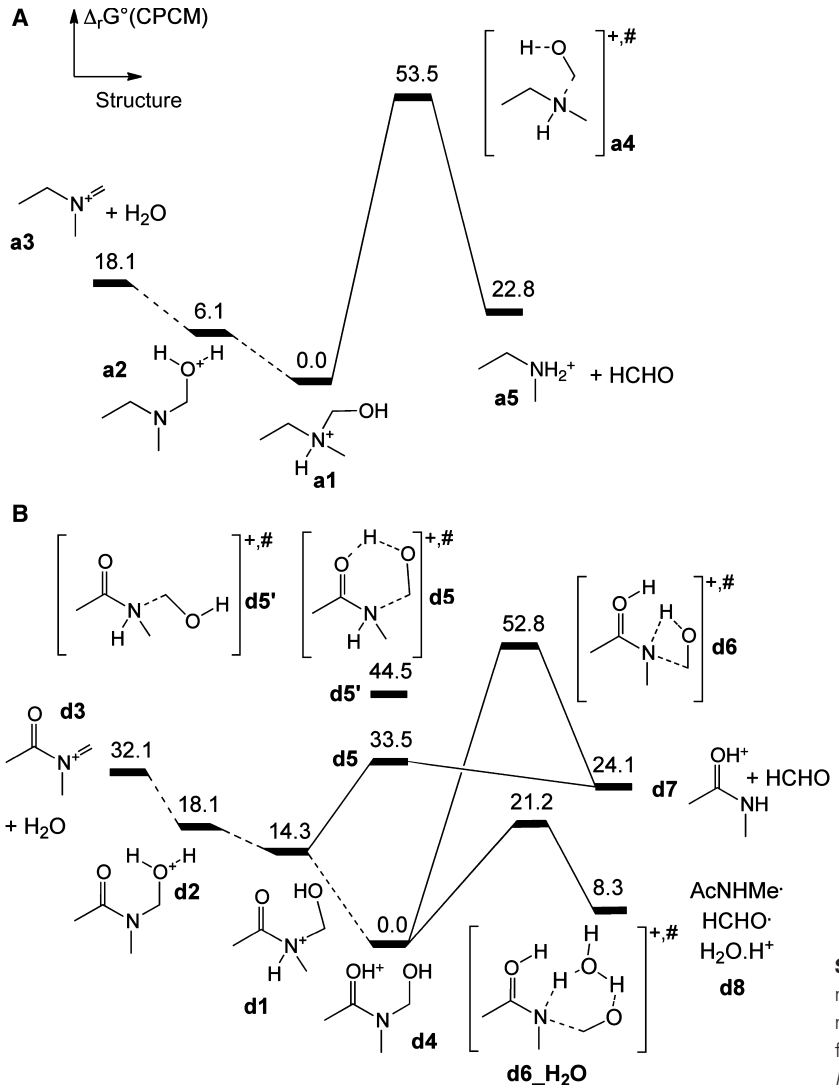

Scheme 4. (A) Free enthalpy profile for the mechanism of deformylation of *N,N,N*-ethyl-methyl-hydroxymethyl-amine. (B) Energy profile for the mechanism of deformylation of *N,N*-methyl-hydroxymethyl-acetamide.

time, the precise identification of a stable carbinol-amide metabolite on a *N*-methylated peptide. This result is even more interesting because *N*-methyl amides are widely used as drugs (e.g. benzodiazepine derivatives) and eventually in peptide structures (e.g. cyclosporins or pristinamycins).

We demonstrated that *N*-carbinol-amide decomposes slowly through deformylation under neutral or mild acidic conditions. The rate of this deformylation reaction is drastically increased under strong acidic or basic conditions, heating or in presence of Lewis base such as a phosphate. Our stability study of carbinol-amide intermediates demonstrates that their lack of detection does not mean that this reactive metabolite is not present in the biological extract. Commonly, incubations are performed in phosphate buffer (pH 7.4) and the analytical protocols involve organic extractions and concentrations, followed by HPLC separation in the presence of acids or bases. In the case of metabolism of TTX and its analogs, we have shown that under such conditions rapid cleavage of the formyl moiety of the carbinol-amide group occurs.

The theoretical study reveals that the stability of carbinol intermediates is governed by the accessibility of the nitrogen lone pair and the pH conditions. Other structural features like cyclic strength have no impact on the stability of such intermediates.

Under neutral conditions, carbinol-amines and carbinol-amides are stable in nonaqueous solution because the energy barriers that need to be reached for deformylation are > 30 kcal·mol^{-1}. If water is present, under neutral or mild basic conditions, energy barriers to deformylation strongly decrease, making deformylation of carbinol-amines an easy transformation. Under

such conditions, deformylation of carbinol-amides occurs more slowly than deformylation of their amino analogs. The increased stability of carbinol-amides compared with carbinol-amines is because of the nitrogen lone pair delocalization in the peptide bond which is active in the deformylation reaction. Under acidic conditions, we were not able to explain the unstability of carbinol-amines; computationally under such conditions, the nitrogen lone pair is protonated and hence prevented deformylation. A more complex scenario involving several protons may be at work in this case. Conversely, for carbinol-amides, among several deformylation pathways, we identified a transition state in which a water molecule assists deformylation. This transition state is lower in energy than that computed under neutral aqueous conditions. Interestingly, the difference in behavior between carbinol-amines and carbinol-amides relies on the accessibility of the nitrogen lone pair, hence the planar NCH_2OH group located between two aromatic groups (carbazole) or between one aromatic and one carbonyl group (nicergoline) should be stable and observable under neutral conditions. In this situation, numerous of conjugated *N*-methylated drugs/prodrugs should yield a stable carbinol intermediate from which biological activities and/or toxicity different from parental NCH_3 or filial NH compounds may arise.

Material and methods

Chemicals

Standard TTX, NADPH, NADP, Glc6*P*, Glc6*P* dehydrogenase and dexamethasone were from Sigma Chemicals (St. Louis, MO, USA). TTX, *iso*-TTX and dihydrotentoxin were kindly provided by B. Liebermann (Iena, Germany). TTX, ^{14}C(Me)-TTX isotopomers and Ala^1-TTX were synthesized as described previously [33,35]. All other chemicals were of the highest quality commercially available.

Preparation of microsomes

Animals were housed and treated according to French legislation in a facility authorized by the Ministry of Agriculture. Male Sprague–Dawley rats (200–220 g; Iffa Credo, St Germain l'Arbresle, France) were treated with dexamethasone (100 mg·kg^{-1} i.p. in corn oil for 3 days). Control rats received only corn oil (0.5 mL·day^{-1} for 3 days). Rats were killed 1 day after the last treatment. Microsomes were prepared from a pool of four to six livers, frozen in liquid nitrogen and stored at −80 °C until use [38]. Human liver samples were kindly provided by the Pharmacology Department of the Besançon University (Besançon, France) and microsomes were prepared as previously described [38].

Quantification of the different enzymes in the microsomal fractions

Protein content in microsomal suspensions was determined by the method of Lowry [39] using BSA as standard. The P450 concentration was measured as described by Omura and Sato [40].

Metabolism

Metabolism of TTX derivatives was studied at 37 °C in 0.1 M phosphate buffer (pH 7.4) with 1.0 μM P450 from liver microsomes of human or rat treated with various inducers using 100.0 μM substrate and an NADPH-generating system (1.0 mM NADP, 10.0 mM Glc6*P* and 2.0 IU Glc6*P* dehydrogenase). The incubation was stopped at the indicated times by addition of the same volume of cold acetonitrile. The mixture was centrifuged at 6000 ***g*** for 10 min and either analyzed after various treatments or stored.

HPLC analysis

Usual HPLC analysis was performed with a linear gradient of eluent on a reverse-phase column (Kromasil 5C$_{18}$, 150 × 4.6 mm). Eluent A, 10% acetonitrile in water; eluent B, 90% acetonitrile in water; gradient, t = 0.0 min 100% A, t = 35.0 min 80% B; flow rate, 1 mL·min^{-1}. In order to specifically improve the HPLC separation of the two metabolites, a gradient of elution was optimized: flow rate, 0.9 mL·min^{-1}; increase in B from 10% at t = 0 to 27% at t = 2 min, then a plateau at 27% to 17 min followed by a linear increase to 29% B to 25 min. In such conditions, M1 and M2 retention times differ by 2 min. We noticed that the presence of acids in the eluent could cause erroneous quantification, and thus their suppression from the eluent was mandatory for a quantitative UV analysis of samples. Indeed, in the presence of acids such as 0.05% trifluoroacetic acid or 0.1% acetic acid in water, the relative amount of M1 decreased dramatically in favor of M2. Metabolites of TTX or *iso*-TTX were detected at 280 nm, those of dihydrotentoxin at 220 nm. Radioactivity was determined by a liquid cell containing a ratio of 50% HPLC eluent to 50% liquid scintillant cocktail (Packard SuperMix™) on a Packard online scintillator. A computer running Waters MILLENNIUM software was used to integrate and calculate the separated peak areas and to plot metabolite patterns.

MS analysis

The HPLC-MS instrument used was an LCQ DUO Ion Trap coupled with an HPLC system from Thermo-Finnigan.

HPLC was performed on a reverse-phase column 150 × 2.1 mm Kromasil $5C_{18}$ column with a linear gradient of eluent at a flow rate of 250 $\mu L \cdot min^{-1}$. Eluent A, 10% acetonitrile in water; eluent B, 90% acetonitrile in water. Twenty microliters of a 50% solution of buffer in CH_3CN was directly injected into the LC system. In a few cases, 0.1% acetic acid was added to eluent A. The program started with 100% of eluent A, then eluent B was increased from 0 to 80% over 25 min and held constant during the next 3 min before returning to initial conditions over 2 min. LC-MS measurements were performed using ESI. ESI was performed at room temperature in negative or positive mode, the voltage was maintained at 4.5 kV and the capillary temperature at 250 °C. It is noteworthy that HPLC-MS performed at high temperature, using APCI or ESI sources, led to degradation of M1 into M2, therefore biasing the analysis. The MS analyzer parameters and collision energy (set at 35%) were optimized on TTX.

NMR analysis

For conformational analysis in $CDCl_3$, proton NMR spectra were recorded using a Bruker Advance 500 spectrometer operating at 500.13 MHz. Spectra were recorded at 300 K, a temperature at which the chemical exchange regime in TTX and its derivatives is either intermediate or fast at the NMR timescale. TMS was used as an internal reference of chemical shift in $CDCl_3$ samples. No pH or temperature correction was used. Spectral processing was done using XWINNMR. 1D spectra were acquired over 32 K data points, using a spectral width of 5 kHz. The relaxation delay was generally 5 s, based on spin-lattice relaxation times measured at low temperature in slow chemical exchange regime.

Computational details

Quantum mechanics calculations were carried out at the DFT-B3PW91 [41,42] level of theory. All atoms were represented by an all-electron, augmented and polarized, triple-ζ quality basis sets 6-311G [43,44]. All the calculations were achieved using the GAUSSIAN 98 suite of programs [45]. Geometries of minima and transition states were fully optimized without any symmetry restriction. Zero point energy and entropic contributions were computed in agreement with the harmonic approximation. Free enthalpies, *G*, were estimated at 298.15 K and 1.0 atm. The connectivity of each transition state was checked while following their intrinsic reaction coordinates. For each molecule, all major conformers were optimized and compared. Only the most stable conformers of the configuration of interest were considered. The nature of the extrema (minima or transition states) were checked using an analytical calculation of the frequencies. Implicit water-solvent corrections were been made according to the CPCM model implemented in GAUSSIAN 98, using Pauling radii and solvent accessible surface.

Acknowledgements

The authors gratefully acknowledge Jean-Marie Gomis (Service de Chimie Bio-Organique et de Marquage, iBiTec-S, CEA-Saclay, France) who achieved the synthesis of radiolabelled tentoxin and their analogs.

References

1 Kedderis GL & Hollenberg PF (1985) Peroxidase-catalyzed N-demethylation reactions: deuterium solvent isotope effects. *Biochemistry* **24**, 6158–6163.
2 Hollenberg PF, Miwa GT, Walsh JS, Dwyer LA, Rickert DE & Kedderis GL (1985) Mechanisms of N-demethylation reactions catalyzed by cytochrome P-450 and peroxidases. *Drug Metab Dispos* **13**, 272–275.
3 Miwa GT, Walsh JS, Kedderis GL & Hollenberg PF (1983) The use of intramolecular isotope effects to distinguish between deprotonation and hydrogen atom abstraction mechanisms in cytochrome P-450- and peroxidase-catalyzed N-demethylation reactions. *J Biol Chem* **258**, 14445–14449.
4 Chen H, de Groot MJ, Vermeulen NPE & Hanzlick RP (1997) Oxidative N-dealkylation of *p*-cyclopropyl-*N*,*N*-dimethylaniline. A substituent effect on a radical-clock reaction rationalized by ab initio calculations on radical cation intermediates. *J Org Chem* **62**, 8227–8230.
5 Shaik S, Kumar D, de Visser SP, Altun A & Thiel W (2005) Theoretical perspective on the structure and mechanism of cytochrome P450 enzymes. *Chem Rev* **105**, 2279–2328.
6 Meunier B, de Visser SP & Shaik S (2004) Mechanism of oxidation reactions catalyzed by cytochrome p450 enzymes. *Chem Rev* **104**, 3947–3980.
7 Niyaz Khan M (1989) Aqueous degradation of *N*-(hydroxymethyl)-phthalimide in the presence of specific and general bases. Kinetic assessment of *N*-hydroxymethyl derivatives of nitrogen heterocycles as possible prodrugs. *J Pharm Biomed Anal* **7**, 685–691.
8 Huizing G, Segura J & Beckett AH (1980) On the mechanism of metabolic N-dealkylation. Isolation of a relatively stable carbinolamine. *J Pharm Pharmacol* **32**, 650–651.
9 Ibe BO & Raj JU (1994) Metabolism of *N*-methylcarbazole by rat lung microsomes. *Exp Lung Res* **20**, 207–222.
10 Kedderis GL, Rickert DE, Pandey RN & Hollenberg PF (1986) ^{18}O studies of the peroxidase-catalyzed oxidation of *N*-methylcarbazole. Mechanisms of carbinolamine and carboxaldehyde formation. *J Biol Chem* **261**, 15910–15914.
11 André V, Boissart C, Sichel F, Gauduchon P, Le Talaer JY, Lancelot JC, Mercier C, Chemtob S, Raoult E & Tallec A (1997) Mutagenicity of nitro- and amino-substituted carbazoles in *Salmonella typhimurium*. III.

Methylated derivatives of 9H-carbazole. *Mutat Res* **389**, 247–260.
12 Kuemmerle SC, Shen T & Hollenberg PF (1994) Inactivation of purified rat liver cytochrome P-450 2B1 and rabbit liver cytochrome P-450 2B4 by *N*-methylcarbazole. *Drug Metab Dispos* **22**, 343–351.
13 Shen T & Hollenberg PF (1994) The mechanism of stimulation of NADPH oxidation during the mechanism-based inactivation of cytochrome P450 2B1 by *N*-methylcarbazole: redox cycling and DNA scission. *Chem Res Toxicol* **7**, 231–238.
14 Yang W, Jiang TR, Davis PJ & Acosta D (1991) *In vitro* metabolism and toxicity assessment of *N*-methylcarbazole in primary cultured rat hepatocytes. *Toxicology* **68**, 217–226.
15 Arcamone F, Glasser AG, Grafnetterova J, Minghetti A & Nicolella V (1972) Studies on the metabolism of ergoline derivatives. Metabolism of nicergoline in man and in animals. *Biochem Pharmacol* **21**, 2205–2213.
16 Shintomi K, Yoshimoto K, Ogawa Y, Itakura T, Ikezawa K, Narita H, Ishizuka T, Yamaguchi I & Yamada K (1987) Pharmacological effects of nicergoline and its metabolites, decomposition products and impurities in animals. *J Pharmacobiodyn* **10**, 35–48.
17 Li Y & Gorrod JW (1994) *N*-Hydroxymethylnorcotinine, a primary *in vitro* metabolite of conitine. *Xenobiotica* **24**, 409–415.
18 Bottiger Y, Dostert P, Benedetti MS, Bani M, Fiorentini F, Casati M, Poggesti I, Alm C, Alvan G & Bertilsson L (1996) Involvement of CYP2D6 but not CYP2C19 in nicergoline metabolism in humans. *Br J Clin Pharmacol* **42**, 707–711.
19 Banno K, Horimoto S & Mabuchi M (1991) Assay of nicergoline and three metabolites in human plasma and urine by high-performance liquid chromatography–atmospheric pressure ionization mass spectrometry. *J Chromatogr* **568**, 375–384.
20 Amato G, Grasso E, Longo V & Gervasi PG (2001) Oxidation of *N*,*N*-dimethylformamide and *N*,*N*-diethylformamide by human liver microsomes and human recombinant P450s. *Toxicol Lett* **124**, 11–19.
21 Kestell P, Gill MH, Threadgill MD, Gescher A, Howarth OW & Curzon EH (1986) Identification by proton NMR of *N*-(hydroxymethyl)-*N*-methylformamide as the major urinary metabolite of *N*,*N*-dimethylformamide in mice. *Life Sci* **38**, 719–724.
22 Hall LR & Hanzlik RP (1990) Kinetic deuterium isotope effects on the N-demethylation of tertiary amides by cytochrome P-450. *Biol Chem* **265**, 12349–12355.
23 Brown KM, von Weymarn LB & Murphy SE (2005) Identification of *N*- (hydroxymethyl) norcotinine as a major product of cytochrome P450 2A6, but not cytochrome P450 2A13-catalyzed cotinine metabolism. *Chem Res Toxicol* **18**, 1792–1798.
24 Iley J & Constantino L (1994) The microsomal dealkylation of *N*,*N*-dialkylbenzamides. *Biochem Pharmacol* **47**, 275–280.
25 Constantino L, Rosa E & Iley J (1992) The microsomal demethylation of *N*,*N*-dimethylbenzamides. Substituent and kinetic deuterium isotope effects. *Biochem Pharmacol* **44**, 651–658.
26 Koike M, Norikura R, Futaguchi S, Yamaguchi T, Sugeno K, Iwatani K, Ikenishi Y & Nakagawa Y (1987) *N*-Hydroxymethyl metabolites of 450191-S, a 1*H*-1,2,4,-triazolyl benzophenone derivative, in dog plasma. *Drug Metab Dispos* **15**, 426–428.
27 Denissen JF, Grabowski BA, Johnson MK, Buko AM, Kempf DJ, Thomas SB & Surber BW (1997) Metabolism and disposition of the HIV-1 protease inhibitor ritonavir (ABT-538) in rats, dogs, and humans. *Drug Metab Dispos* **25**, 489–501.
28 Jegorov A, Halada P & Safarcik K (2000) Cyclosporin A metabolism in brown bullhead, *Ameriurus nebulosus*. *Fish Physiol Biochem* **23**, 257–264.
29 Avni A, Anderson JD, Holland N, Rochaix JD, Gromet-Elhanan Z & Edelman M (1992) Tentoxin sensitivity of chloroplasts determined by codon 83 of β subunit of proton-ATPase. *Science* **257**, 1245–1247.
30 Minoletti C, Santolini J, Haraux F, Pothier J & André F (2002) Rebuilt 3D structure of the chloroplast F1 ATPase–tentoxin complex. *Proteins* **49**, 302–320.
31 Santolini J, Minoletti C, Gomis JM, Sigalat C, André F & Haraux F (2002) An insight into the mechanism of inhibition and reactivation of the F(1)-ATPases by tentoxin. *Biochemistry* **41**, 6008–6018.
32 Delaforge M, André F, Jaouen M, Dolgos H, Benech H, Gomis JM, Noel JP, Cavelier F, Verducci J, Aubagnac JL *et al*. (1997) Metabolism of tentoxin by hepatic cytochrome P-450 3A isozymes. *Eur J Biochem* **250**, 150–157.
33 Loiseau N, Cavelier F, Noel JP & Gomis JM (2002) High yield synthesis of tentoxin, a cyclic tetrapeptide. *J Peptide Sci* **8**, 335–346.
34 Pinet E, Neumann JM, Dahse I, Girault G & André F (1995) Multiple interconverting conformers of the cyclic tetrapeptide tentoxin, [cyclo-(L-MeAla^1-L-Leu^2-MePhe[(Z)-Δ]^3-Gly^4)], as seen by two-dimensional ^{1}H-NMR spectroscopy. *Biopolymers* **36**, 135–152.
35 Pinet E, Gomis JM, Girault G, Cavelier F, Verducci J, Noel JP & André F (1996) Tentoxin has at least two binding sites on CF1 and epsilon-depleted CF1 ATPases isolated from spinach chloroplast. *FEBS Lett* **395**, 217–220.
36 Wang Y, Kumar D, Yang C, Han K & Shaik S (2007) Theoretical Study of N-demethylation of substituted *N*,*N*-dimethylanilines by cytochrome P450: the mechanistic significance of kinetic isotope effect profiles. *J Phys Chem B* **111**, 7700–7710.

37 Schyman P, Usharani D, Wang Y & Shaik S (2010) Brain chemistry: how does P450 catalyze the O-demethylation reaction of 5-methoxytryptamine to yield serotonin? *J Phys Chem B*, **114**, 7078–7089.
38 Kremers P, Beaune P, Cresteil T, de Graeve J, Columelli S, Leroux JP & Gielen JE (1981) Cytochrome P-450 monooxygenase activities in human and rat liver microsomes. *Eur J Biochem* **118**, 599–606.
39 Lowry OH, Rosebrough NJ, Farr AL & Randall RJ (1951) Protein measurement with the Folin phenol reagents. *J Biol Chem* **193**, 265–275.
40 Omura T & Sato R (1964) The carbon monoxide-binding pigment of liver microsomes. I. Evidence for its hemoprotein nature. *J Biol Chem* **239**, 2370–2378.
41 Becke AD (1993) Density-functional thermochemistry. III. The role of exact exchange. *J Chem Phys* **98**, 5648–5652.
42 Perdew JP & Wang Y (1992) Accurate and simple analytic representation of the electron–gas correlation-energy. *Phys Rev B* **45**, 13244–13249.
43 McLean AD & Chandler GS (1980) Contracted gaussian-basis sets for molecular calculations. I. Second row atoms, Z = 11–18. *J Chem Phys* **72**, 5639–5648.
44 Krishnan R, Binkley JS, Seeger R & Pople JA (1980) Self-consistent molecular-orbital methods. XX. Basis set for correlated wave-functions. *J Chem Phys* **72**, 650–654.
45 Frisch MJ, Trucks GW, Schlegel HB, Scuseria GE, Robb MA, Cheeseman JR, Zakrzewski VG, Montgomery JA Jr, Stratmann RE, Burant JC *et al.* (2001) Gaussian 98 (Revision A.11), Gaussian, Inc., Pittsburgh PA, 2001.

Supporting information

The following supplementary material is available:
Doc. S1. Cartesian coordinates, energy, enthalpy, free enthalpy and free enthalpy in solution of each compound optimized together with 3D representations of key transition states and their main distances.

This supplementary material can be found in the online version of this article.

Please note: As a service to our authors and readers, this journal provides supporting information supplied by the authors. Such materials are peer-reviewed and may be re-organized for online delivery, but are not copy-edited or typeset. Technical support issues arising from supporting information (other than missing files) should be addressed to the authors.